ELSEVIER

Advances in Water Resources 23 (2000) 637–643

Advances in Water Resources

The simulation of dam-break flows by an improved predictor–corrector TVD scheme

Ming Hseng Tseng [a], Chia R. Chu [b,*]

[a] Department of Information Management, Ling Tung College and National Center for High-Performance Computing, Taiwan, ROC
[b] Department of Civil Engineering, National Central University, Taiwan 32054, ROC

Received 15 December 1998; accepted 20 November 1999

Abstract

This paper reports a finite difference predictor–corrector TVD (total variation diminishing) scheme for the computation of unsteady one-dimensional dam-break flows. The algorithm modified the widely used MacCormack scheme by implementing a conservative dissipation step to avoid any unphysical oscillation in the vicinity of strong gradients in the numerical solution. A general treatment for satisfying the entropy inequality condition is incorporated. The accuracy and robustness of the numerical scheme are verified with an analytic solution and experimental data. Furthermore, a sensitivity study is carried out to investigate the accuracy of four different versions of the predictor–corrector schemes. It is found that the numerical scheme will have less computational error and higher efficiency when the direction of the predictor–corrector step is the same as the direction of the shock wave propagation.

Keywords: Finite difference; Predictor–corrector TVD scheme; Dam-break flows

1. Introduction

The prediction of dam-break flows is of great interest to hydraulic engineers. Variations of water depths and velocities in these extreme events are important parameters for the design of hydraulic systems and for flood control operations. However, it is well known that numerical simulations for such flows are difficult, because of the steep gradient inherent in the problem. Early works on dam-break simulations involved using the method of characteristics and shock fitting techniques [1]. However, most of these traditional simulation models display spurious oscillations at the shock fronts.

More recently, a number of shock-capturing schemes for solving the St. Venant equations have been proposed. For instance, Fennema and Chaudhry [2,3] used the MacCormack model along with the Beam-Warming scheme to simulate one-dimensional and two-dimensional dam-break flows. Rahman and Chaudhry [4] combined the MacCormack scheme and an adaptive grid technique to calculate such flows. However, their models require an empirical artificial viscosity term to damp out the oscillation around the discontinuities. The choice of this artificial viscosity requires both fine-tuning and adapt judgement.

Harten [5] introduced the notion of total variation diminishing (TVD) to solve hyperbolic equations. This TVD scheme not only has the ability to damp out the oscillation, but also does not contain terms with adjustable parameters. Garcia-Navarro et al. [6] combined MacCormack's [7] explicit scheme and the TVD technique to simulate unsteady open channel flows. Their scheme does not cause any additional difficulty when dealing with the source terms of the equation and retains second-order accuracy in both space and time.

In this study, the predictor–corrector TVD scheme proposed by Garcia-Navarro et al. [6] is extended to include four versions of the predictor–corrector steps. Also, the entropy correction function suggested by Harten and Hyman [8] is used to eliminate the trial procedure for the entropy inequality condition. Simulation results from the present model are verified with an analytical solution and experimental data. Then, a sensitivity study is carried out to investigate the accuracy and efficiency of the predictor–corrector schemes. As well, the model is utilized to study the effect of the channel roughness and the initial depth ratio on the propagation speed of the shock wave.

* Corresponding author. Tel.: +886-3-427-9127; fax: +886-3-427-9127.
E-mail address: crchu@cc.ncu.edu.tw (C.R. Chu).

0309-1708/00/$ - see front matter
PII: S0309-1708(99)00051-2

2. Governing equations

Based on the hydrostatic pressure distribution and small channel slope assumptions, an unsteady open channel flow can be described by the St. Venant equations. Shallow water flows can be described in conservative form as

$$\frac{\partial Q}{\partial t}+\frac{\partial F}{\partial x}=S, \tag{1}$$

where t represents time, x represents longitudinal distance,

$$Q=\begin{bmatrix} h \\ uh \end{bmatrix} \tag{2}$$

and

$$F=\begin{bmatrix} uh \\ u^2h+\frac{gh^2}{2} \end{bmatrix}, \tag{3}$$

where h is the water depth, u the depth-averaged velocity, respectively, and g the gravitation acceleration. The source term S in Eq. (1) includes the effect due to bottom slope and friction

$$S=\begin{bmatrix} 0 \\ gh(S_o-S_f) \end{bmatrix}, \tag{4}$$

where S_o is the slope of the channel bottom, and S_f is the slopes of the energy grade line,

$$S_f=\frac{n^2u^2}{R^{4/3}}, \tag{5}$$

n is the Manning coefficient, and R the hydraulic radius.

Eq. (1) can be expressed in quasi-linear form as

$$\frac{\partial Q}{\partial t}+A\frac{\partial Q}{\partial x}=S, \tag{6}$$

where A is the Jacobian matrix having two real eigenvalues

$$\lambda_1=u+c, \quad \lambda_2=u-c, \tag{7}$$

where $c=\sqrt{gh}$ is the wave celerity. In this study, the corresponding right and left eigenvector matrices for matrix A are defined as

$$R=h\begin{bmatrix} 1 & 1 \\ \lambda_1 & \lambda_2 \end{bmatrix} \quad \text{and} \quad L=\frac{1}{2hc}\begin{bmatrix} -\lambda_2 & 1 \\ \lambda_1 & -1 \end{bmatrix}. \tag{8}$$

For the hyperbolicity, the Jacobian matrix A can be found

$$A=R\Lambda L, \quad \Lambda=\begin{bmatrix} \lambda_1 & 0 \\ 0 & \lambda_2 \end{bmatrix}. \tag{9}$$

3. Predictor–corrector TVD scheme

The computational domain is discretized as $x_i=i\Delta x$ and $t^n=n\Delta t$, where Δx is the size of a uniform mesh, and Δt is the time increment. The present scheme is based on a predictor–corrector three-step procedure. The first two steps follow the algorithm suggested by Garcia-Navarro et al. [6]

$$Q_i^{\mathrm{p}}=Q_i^n-\tau\left(F_{i+1}^n-F_i^n\right)+\Delta tS_i^n, \tag{10}$$

$$Q_i^{\mathrm{c}}=Q_i^n-\tau\left(F_i^p-F_{i-1}^p\right)+\Delta tS_i^p. \tag{11}$$

The third step equips the algorithm with the dissipation property of the TVD scheme

$$Q_i^{n+1}=\frac{1}{2}\left(Q_i^{\mathrm{p}}+Q_i^{\mathrm{c}}\right)+\frac{1}{2}\left(R_{i+\frac{1}{2}}\Phi_{i+\frac{1}{2}}-R_{i-\frac{1}{2}}\Phi_{i-\frac{1}{2}}\right), \tag{12}$$

where $\tau=\Delta t/\Delta x$ is the mesh ratio and the superscript p and c stand for the predictor and the corrector step, respectively. The subscript $\left(i+\frac{1}{2}\right)$ denotes the intermediate state between grid points (i) and $(i+1)$. The $\Phi_{i+\frac{1}{2}}$ component in Eq. (12) is defined as

$$\Phi_{i+\frac{1}{2}}^k=\psi\left(\lambda_{i+\frac{1}{2}}^k\right)\left(1-\tau\left|\lambda_{i+\frac{1}{2}}^k\right|\right)\left(1-\varphi\left(r_{i+\frac{1}{2}}^k\right)\right)\alpha_{i+\frac{1}{2}}^k, \tag{13}$$

where the index $k=1$ and 2. The entropy correction function ψ in Eq. (13) is defined as

$$\psi(z)=\begin{cases} |z| & \text{if } |z|\geqslant\varepsilon, \\ \varepsilon & \text{if } |z|<\varepsilon. \end{cases} \tag{14}$$

For this study, a formula suggested by Harten and Hyman [8] is used to calculate ε

$$\varepsilon_{i+\frac{1}{2}}^k=\max\left[0, \quad \lambda_{i+\frac{1}{2}}^k-\lambda_i^k, \quad \lambda_{i+1}^k-\lambda_{i+\frac{1}{2}}^k\right]. \tag{15}$$

The characteristic variable α in Eq. (13) is defined as

$$\alpha_{i+\frac{1}{2}}=L_{i+\frac{1}{2}}(Q_{i+1}-Q_i). \tag{16}$$

The purpose of the flux limiter function φ in Eq. (13) is to supply artificial dissipation when there is a discontinuity or a strong gradient, while adding very little or no dissipation in regions of smooth variation. Hirsch [10], Roe [11] and Sweby [12] have suggested different models for the function φ. In this study, the φ function of Yee [9] was used

$$\varphi\left(r_{i+\frac{1}{2}}^k\right)=\frac{r_{i+\frac{1}{2}}^k+\left(r_{i+\frac{1}{2}}^k\right)^2}{1+\left(r_{i+\frac{1}{2}}^k\right)^2}, \tag{17}$$

where

$$r_{i+\frac{1}{2}}^k=\frac{\alpha_{i+\frac{1}{2}-\sigma}^k}{\alpha_{i+\frac{1}{2}}^k} \quad \text{and} \quad \sigma=\operatorname{sign}\left(\lambda_{i+\frac{1}{2}}^k\right). \tag{18}$$

Following the technique suggested by Roe [11], the mean values of velocity and water depth can be calculated as follows:

$$u_{i+\frac{1}{2}}=\frac{\sqrt{h_i}u_i+\sqrt{h_{i+1}}\,u_{i+1}}{\sqrt{h_i}+\sqrt{h_{i+1}}}, \tag{19}$$

$$c_{i+\frac{1}{2}}=\sqrt{\frac{g(h_i+h_{i+1})}{2}}. \tag{20}$$

Due to the fact that the MacCormack scheme incorporates forward and backward differences in separated predictor and corrector steps, an alternative would be to reverse the order of the predictor and corrector steps:

$$Q_i^{\mathrm{p}} = Q_i^n - \tau\left(F_i^n - F_{i-1}^n\right) + \Delta t S_i^n, \tag{21}$$

$$Q_i^{\mathrm{c}} = Q_i^n - \tau\left(F_{i+1}^p - F_i^p\right) + \Delta t S_i^p. \tag{22}$$

In this study, four possible combinations are adopted to investigate the robustness of the TVD scheme for dam-break flow simulations. The four different schemes are denoted as follows: the Forward–Backward (F–B) scheme combines Eqs. (10)–(12); the Backward–Forward (B–F) scheme combines Eqs. (21), (22) and (12); the Forward–Backward-cycled (F–B-C) scheme combines Eqs. (10)–(12), (21), (22) and (12) in a cyclic manner; and the Backward–Forward-cycled (B–F-C) scheme combines Eqs. (21), (22), (12), (10)–(12) in a cyclic manner.

In order to satisfy the numerical stability requirement, the time step is determined based on the Courant–Friedrich–Lewy criterion [13]

$$\Delta t = Cr\left[\frac{\Delta x}{u+c}\right], \tag{23}$$

where Cr is the Courant number. Neumann boundary condition ($\mathrm{d}h/\mathrm{d}x = 0$) is applied to the water depth at the inlet and outlet boundaries. The velocities at the boundaries are obtained by solving the Riemann invariant problem ([1, 10]).

4. Model verification

In order to demonstrate that the proposed scheme is capable of describing dam-break flows, model predictions are compared with exact solutions and the results of laboratory experiment as described in the following.

4.1. An idealized dam-break flow

The first test case of the proposed scheme is an idealized dam-break flow in a rectangular, frictionless channel. Fig. 1 shows a schematic diagram of the problem, where h_{r} and h_{t} are the initial water depths in the reservoir and in the tail water, respectively. At time $t = 0$, the dam is removed instantaneously and the water is released to the downstream side in the form of a shock wave. Based on the geometry and upstream condition, an analytic solution can be found [14]. In this study, the design of the simulation conditions is similar to that of Rahman and Chaudhry [4]. The computation domain is comprised of a 2000 m long channel with a horizontal channel bottom. The dam is located at the downstream distance $x = 1025$ m. The initial water depth in the reservoir is $h_{\mathrm{r}} = 10$ m. The flow domain is discretized into

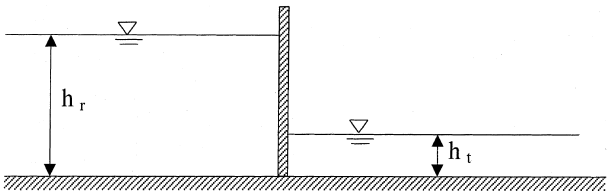

Fig. 1. Schematic diagram of a dam-break flow.

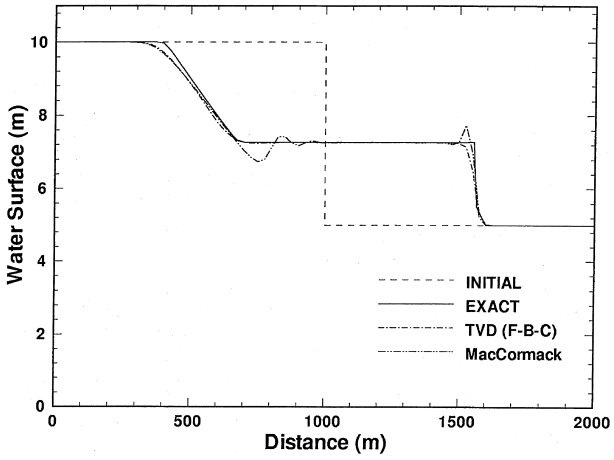

Fig. 2. Computed and analytical solutions for an idealized dam-break flow at time $t = 60$ s.

80 uniform grids. The time evolution of the water depth can be used to examine the shock-capturing capability of the numerical scheme.

Fig. 2 shows the water depth variations along the channel for a dam-break flow with a depth ratio of $h_{\mathrm{t}}/h_{\mathrm{r}} = 0.5$ at time $t = 60$ s. The result of the Forward–Backward-Cycled (F–B-C) scheme is compared with the exact solution to demonstrate the robustness of the proposed TVD scheme. The comparison between four different schemes will be shown in Section 5. The water depth, simulated by a finite-difference MacCormack scheme, is also plotted in Fig. 2 for comparison. It clearly shows that the proposed TVD scheme faithfully captures the shock wave, while the traditional MacCormack scheme has an unphysical oscillation at the shock front. Also, when compared with the numerical results of Rahman and Chaudhry [4], our TVD scheme does not need to employ an adaptive grid to obtain oscillation-free shock waves.

4.2. Dam-break experiment

The above test case only compares the simulation results with the analytic solution. In order to demonstrate that the proposed scheme is capable of describing a real dam-break scenario, the laboratory dam-break experiments of Waterway Experiment Station (WES), US Corps of Engineers [15] are also simulated in this study. The experiments were conducted in a rectangular

channel with length of 122 m, width of 1.22 m, bottom slope of 0.005, and the Manning coefficient $n = 0.0085$. The water depth upstream of the dam is 0.305 m, and the downstream water depth is zero (dry bed). The flow domain is discretized into 122 grids with a uniform grid spacing $\Delta x = 1.0$ m. Fig. 3(a) shows a comparison of the computed and measured water depth variations along the centerline of the flume at time $t = 10$ s. Figs. 3(b) and (c) compare the simulated water depth with the experimental data at downstream distances $x = 70.1$ m and $x = 85.4$ m, respectively. The good agreement between the computed and measured water depth ascertains that the proposed TVD scheme is capable of dam-break flow simulations.

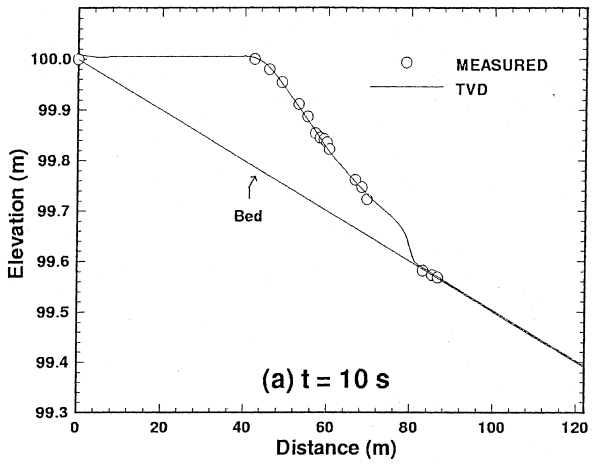

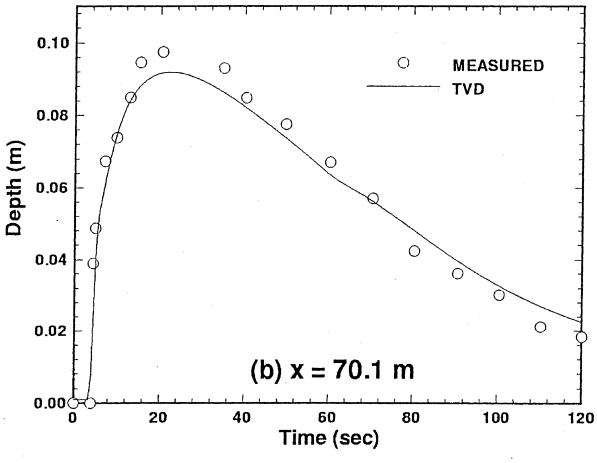

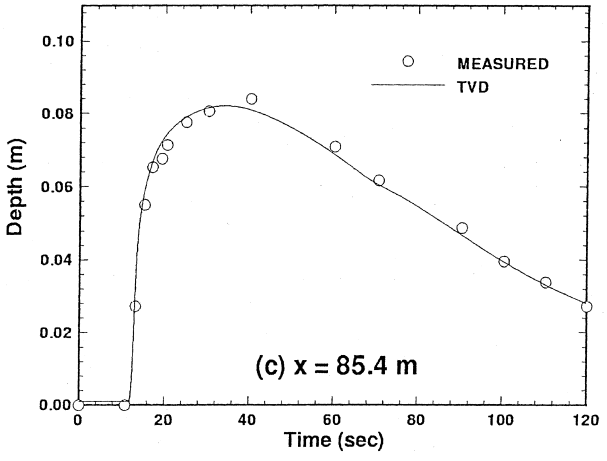

Fig. 3. Comparison of computed and experimental results for a dam-break flow. (a) at time $t = 10$ s; (b) $x = 70.1$ m; (c) $x = 85.4$ m.

5. Results and discussion

In this section, the efficiency and robustness of four versions of the predictor–corrector schemes are investigated. The design of simulation conditions is similar to the configuration used by Rahman and Chaudhry [4]. The water depths predicted by the four different schemes, namely F–B, B–F, F–B-C, and B–F-C schemes, for a subcritical flow ($h_t/h_r = 0.5$ at time $t = 60$ s) are shown in Fig. 4. This comparison clearly shows that all four TVD schemes can accurately predict the shock wave without spurious oscillations. The water depth simulated by the MacCormack scheme is also plotted in Fig. 4 for comparison. It clearly shows that the proposed TVD scheme faithfully captures the shock wave, while the traditional MacCormack scheme has an unphysical oscillation at the shock front.

Table 1 summarizes a quantitative comparison of the relative error between the simulated and analytic solutions. The relative error is defined by the L_2 norm

$$L_2 = \left[\sum \left(Y_i^{\text{cal}} - Y_i^{\text{exact}}\right)^2 \Big/ \sum \left(Y_i^{\text{exact}}\right)^2\right]^{1/2}, \qquad (24)$$

where Y_i^{cal}, Y_i^{exact} are the simulated and exact solution at grid point (i). As can be seen in Table 1, the errors in all four TVD schemes are smaller than for the MacCormack scheme. But the differences between the TVD schemes are not significant enough. The Courant numbers Cr are set to be 0.95 in all the schemes for this simulation. The value of Cr is an indicator of the efficiency of the numerical scheme. As the value of Cr increases, the efficiency of the numerical scheme increases.

In order to illustrate the difference between the TVD schemes, a super-critical dam-break flow ($h_t/h_r = 0.004$) is simulated. The predicted water depth at time $t = 60$ s is shown in Fig. 5. The B–F-C and B–F schemes failed to capture the shock front. Besides that, the agreement between the simulation results and the exact solution is satisfactory, considering the traditional MacCormack scheme failed to compute the same case. As can be seen in Table 1, the relative errors of the F–B and F–B-C schemes are smaller than that of the B–F and B–F-C schemes. The highest values of Cr can be used for the B–F and B–F-C schemes are 0.25, while the values of Cr for the F–B and F–B-C schemes are 0.95. This implies that

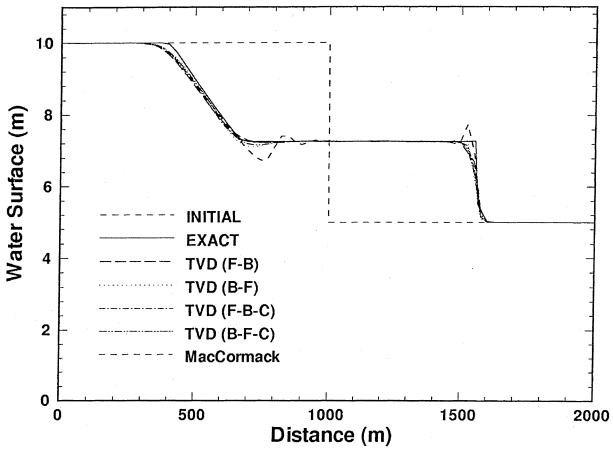

Fig. 4. Water depth variation for a depth ratio of $h_t/h_r = 0.5$ at time $t = 60$ s.

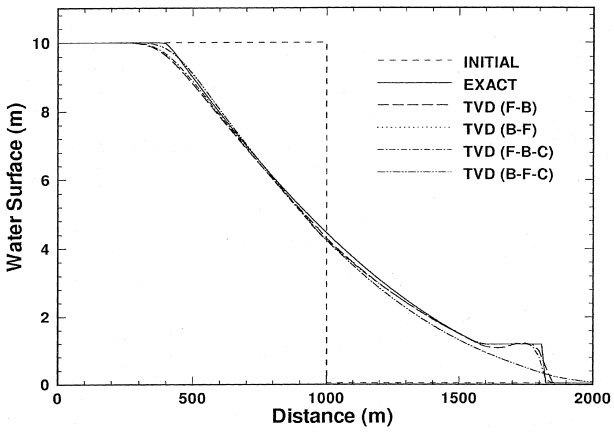

Fig. 5. Water depth variation for a depth ratio of $h_t/h_r = 0.004$ at time $t = 60$ s.

the F–B and F–B-C schemes have a better computational efficiency for this case ($h_t/h_r = 0.004$).

The directional dependence of the predictor–corrector schemes is investigated by reversing the water depths in the reservoir and the tail water. In other words, the depth ratio is $h_t/h_r = 250$ and the shock wave propagates from right to left. The computational results are shown in Fig. 6 and Table 1. Fig. 6 is similar to Fig. 5 except that the direction of the shock wave is reversed and the F–B-C and B–F schemes failed to capture the shock front. Table 1 indicates that the relative errors of the F–B and F–B-C schemes are larger than that of the B–F and B–F-C schemes for the reversed case. Furthermore, the values of *Cr* suggest that the B–F and B–F-C schemes have a better efficiency for this case.

This sensitivity study indicates that when the direction of the predictor–corrector step is the same as the shock wave propagation, the simulation will have less computational error and a higher efficiency. Therefore, the choice of numerical scheme should depend on the direction of the shock wave propagation. Table 1 also indicates that the errors for the cyclic schemes are smaller that for the corresponding non-cyclic schemes by a tiny margin. Nevertheless, the accumulation of initial error caused by the directional dependence can not be attenuated by the cyclic procedure if the direction of the numerical scheme is different from the direction of the shock wave.

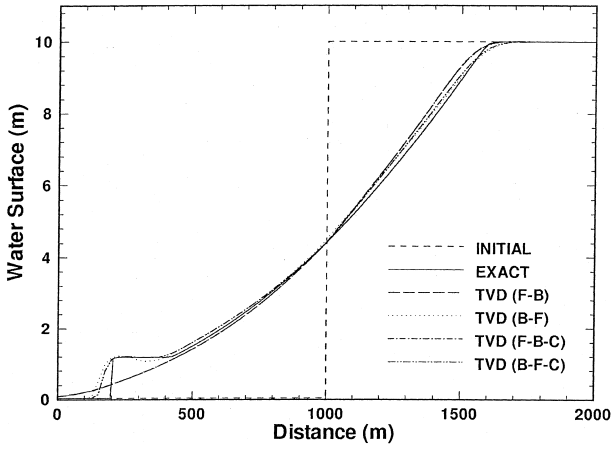

Fig. 6. Water depth variation for a depth ratio of $h_t/h_r = 250$ at time $t = 60$ s.

The F–B predictor–corrector scheme is adopted to study the effect of the depth ratio h_t/h_r on the propagation speed of shock waves. Figs. 7(a) and (b) show the water depth variation for subcritical and supercritical dam-break flows, respectively. This comparison clearly indicates that the propagation speed increases as the depth ratio decreases in supercritical dam-break flows (Fig. 7(b)). However, this phenomenon is not notable in subcritical flows (Fig. 7(a)) because the difference in the depth ratio is small.

Table 1
Simulation results for dam-break flows

Depth ratio		$h_t/h_r = 0.5$		$h_t/h_r = 0.004$		$h_t/h_r = 250$	
Schemes		*Cr*	L_2 (%)	*Cr*	L_2 (%)	*Cr*	L_2 (%)
TVD scheme	F–B	0.95	1.48	0.95	2.00	0.25	3.70
	B–F	0.95	1.68	0.25	3.90	0.95	2.70
	F–B-C	0.95	1.48	0.95	1.80	0.25	3.60
	B–F-C	0.95	1.53	0.25	3.90	0.95	2.30
MacCormack scheme		0.95	1.81	×	×	×	×

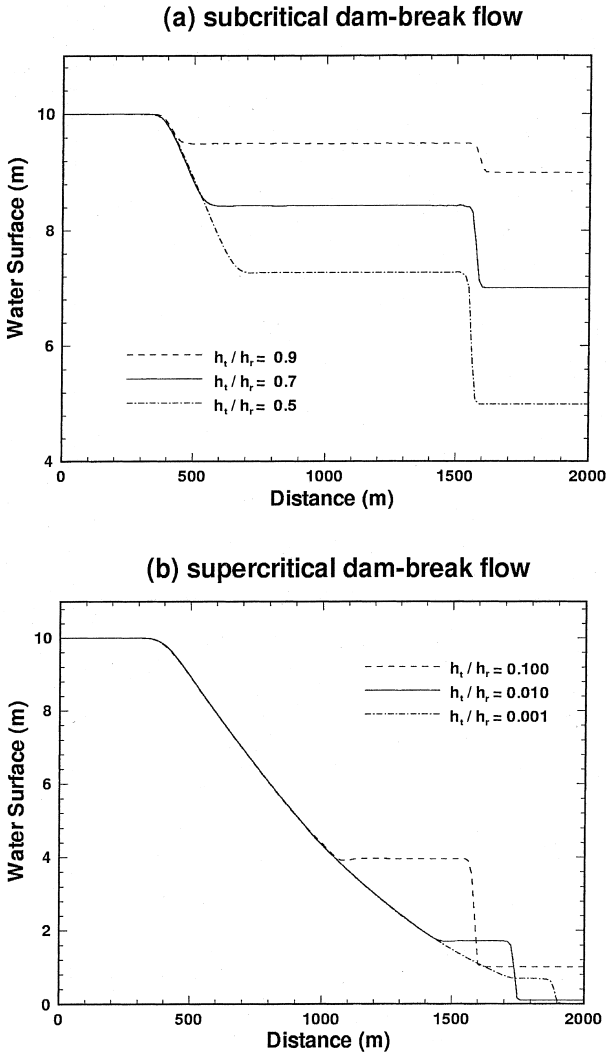

Fig. 7. Water depth variation at time $t = 60$ s. (a) subcritical dam-break flow and (b) supercritical dam-break flow.

The present scheme does not cause any additional difficulty when dealing with the source term. Therefore, it is utilized to examine the influence of channel roughness (Manning coefficient n) on the shock wave. Fig. 8 shows the results for a depth ratio of $h_t/h_r = 0.01$, for $n = 0.0, 0.02$, and 0.04 at a time of $t = 60$ s. As expected, the propagation speed decreases as the value of n (bottom friction) increases. This comparison also demonstrates the error of neglecting the channel roughness in flood routing.

It is important to inspect the behavior of a numerical scheme over a range of grid size. Fig. 9 illustrates the simulated water depths of a supercritical dam-break flow $h_t/h_r = 0.004$ using different numbers of grid points (NP). The F–B numerical algorithm is used while the value of Cr is set to be 0.95 for all the runs. As the grid point number increases, the shock fronts become steeper and the water depth profiles become closer to the analytic solution. A quantitative comparison of the above

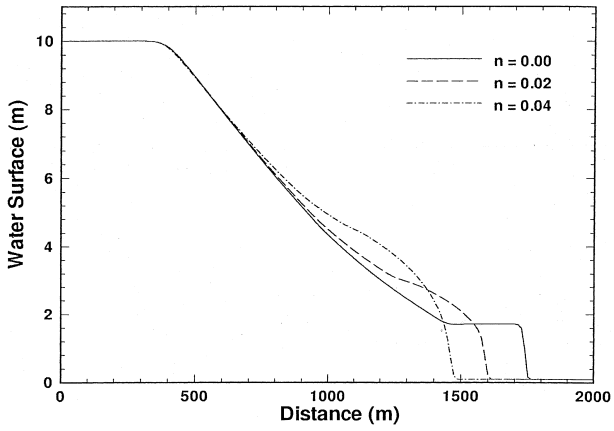

Fig. 8. Effect of Manning coefficient on shock wave propagation.

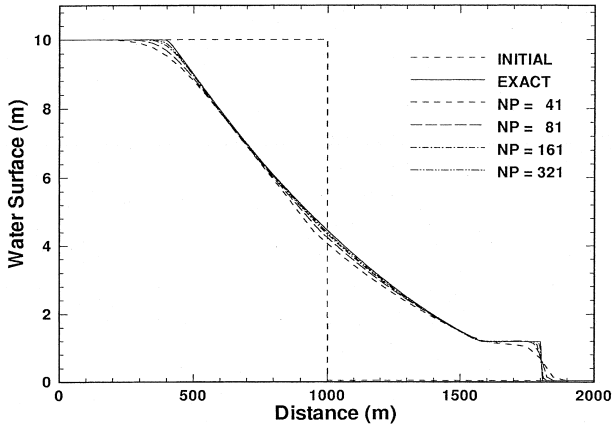

Fig. 9. Effect of grid size on dam-break flows.

results can be found in Table 2. The CPU time was counted on a PC 586 computer. Here the relative error $|E|$ is also calculated as

$$|E| = \left[\sum_{i=1}^{NP}\left(Y_i^{cal} - Y_i^{exact}\right)^2\right]^{1/2} \tag{25}$$

in order to compare with the computational error using the MacCormack scheme and an adaptive grid [4]. This comparison evidently demonstrates that the proposed TVD scheme can acquire remarkable accuracy even with a uniform grid. Furthermore, the results in Table 2 indicate that the computational error decreases as the number of grid points increases.

Table 2
Simulation results for a depth ratio of $h_t/h_r = 0.004$

Grid point	Δx (m)	L_2 (%)	$\|E\|$	CPU time (s)
41	50	3.27	1.302	2.0
81	25	1.84	1.024	3.0
161	12.5	1.07	0.846	3.5
321	6.25	0.57	0.628	6.0

6. Conclusions

A finite-difference predictor–corrector TVD scheme is developed to simulate one-dimensional dam-break flows. This algorithm modifies the widely used MacCormack scheme by implementing a conservative dissipation step according to the theory of total variation diminishing (TVD) to avoid the spurious oscillation. The accuracy and robustness of the proposed model are verified with an analytic solution and experimental data. The efficiency and robustness of four different versions of the predictor–corrector scheme, namely the Forward–Backward (F–B), the Backward–Forward (B–F), the Forward–Backward-cycled (F–B-C), and the Backward–Forward-cycled (B–F-C) schemes are investigated. Based on the results of this study, several conclusions can be made:

1. The accuracy and robustness of the proposed TVD scheme compare favorably than that of the traditional MacCormack scheme for dam-break flow simulation.
2. The numerical scheme has less computational error and a higher efficiency when the direction of the predictor–corrector step is in the same direction as the shock wave propagation.
3. The simulation results demonstrate that the errors of the cyclic schemes are smaller that the non-cyclic schemes. But the accumulation of initial errors caused by the directional dependence cannot be eliminated by the cyclic schemes.
4. The propagation speed of the shock wave increases as the depth ratio decreases in supercritical dam-break flows. Also, the propagation speed decreases as the channel friction (Manning coefficient n) increases.
5. The computational error decreases as the number of grid points increases. The computational time increases as the grid points increase, but the difference is not very significant.

References

[1] Chaudhry MH. Open-channel flow. Englewood Cliffs, NJ: Prentice-Hall, 1993.
[2] Fennema RJ, Chaudhry MH. Simulation of one-dimensional dam-break flows. J Hydraulic Res 1987;25:41–51.
[3] Fennema RJ, Chaudhry MH. Explicit methods for 2-D transient free-surface flows. J Hydraulic Eng ASCE 1990;116(8):1013–35.
[4] Rahman M, Chaudhry MH. Simulation of dam-break flow with grid adaptation. Adv Water Res 1998;21(1):1–9.
[5] Harten A. High resolution schemes flow hyperbolic conservation laws. J Comp Phys 1983;49:357–93.
[6] Garcia-Navarro P, Alcrudo F, Saviron JM. 1-D open channel flow simulation using TVD-MacCormack scheme. J Hydraulic Eng, ASCE 1992;118(10):1359–72.
[7] MacCormack RW. The effect of viscosity in hyper-velocity scatering. AIAA, Paper No. 69-354. Washington: DC, 1969.
[8] Harten A, Hyman P. Self-adjusting grid methods for one-dimensional hyperbolic conservation laws. J Comp Phys 1983;50:235–69.
[9] Yee HC. A class of high-resolution explicit and implicit shock-capturing methods. NASA TM-101088, 1989.
[10] Hirsch C. Numerical computation of internal and external flows: vol. 2: Computational Methods for Inviscid and Viscous Flows, Wiley, New York, 1988.
[11] Roe PL. Approximate Riemann solvers parameter vectors and different schemes. J Comput Phys 43;1981:357–72.
[12] Sweby PK. High resolution schemes using flux limiters hyperbolic conservation laws. SIAM J Numer Anal 1984;21(5):995–1011.
[13] Courant R, Friedrich KO, Lewy H. On the partial differential equation of mathematical physics. IBM J 1967;11(2):215–34.
[14] Stoker JJ. Water waves: Mathematical theory with applications, Wiley-Interscience, Singapore, 1958.
[15] US Corps of Engineers, Flood resulting from suddenly breached dams, Miscellaneous paper, 2 (374), Report 1, US Army Engineer Waterways Experiment Station, Corps of Engineers, Vicksburg, Mississippi, 1960.